ACS OMEGA

Open Access



http://pubs.acs.org/journal/acsodf

Article

# Antifouling Zwitterionic Nanofibrous Wound Dressing for Long-Lasting Antibacterial Photodynamic Therapy

Wen-Yen Chang and Ching-Yi Chen*

Cite This: *ACS Omega* 2023, 8, 36906−36918

Read Online

ACCESS | Metrics & More | Article Recommendations | Supporting Information

**ABSTRACT:** Nanofibrous mats as a wound dressing have received great attention in recent year. The development of biocompatible dressings with antibiofouling capability and long-lasting antibacterial properties is important but challenging. Antibacterial photodynamic therapy (aPDT) effectively eliminates pathogens via a photodynamic process that can circumvent the emergence of antibiotic-resistant pathogens. In this study, we integrated the zwitterionic materials (2-methacryloyloxyethyl phosphorylcholine (MPC) moiety) and aPDT photosensitizer, methylene blue (MB), to fabricate a long-lasting antibacterial nanofibrous mat using electrospinning technology. The prepared nanofibers possessed an appropriate water absorption and retention ability, superior cytocompatibility, and antibiofouling ability against both proteins and L929 cell adhesion. MB-loaded nanofibrous mats have exhibited superior aPDT against Gram-positive *Staphylococcus aureus* compared to Gram-negative *Escherichia coli* under moderate irradiation (100 W $m^{-2}$) due to the presence of an extra outer membrane of Gram-negative bacteria serving as a protective barrier. In vitro release study demonstrated that the nanofibrous mat had a long-lasting drug release profile, which can efficiently suppress bacterial growth via aPDT. The antibacterial ability of the MB-loaded nanofibrous mat was commensurate or slightly inferior to antibiotics such as tetracycline and kanamycin, suggesting that it has the potential to be used as an antibiotic alternative. Overall, this zwitterionic nanofibrous mat with long-lasting aPDT function and nonadherent properties has potential as a promising antibacterial wound dressing.

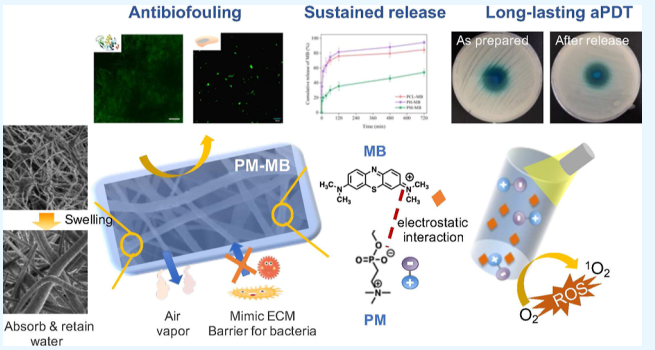


## 1. INTRODUCTION

Skin is the first physical barrier of the human immune system to resist the invasion of external pathogens. Once injured, external bacteria may invade and cause infection and inflammation of the wound.[1] Therefore, an appropriate wound dressing is essential and should be carefully selected in accordance with the type of wound in order to facilitate wound healing. During the stage of wound repair, protein-rich fluids are secreted for tissue repair, immune cell activation, and blood clotting. Traditional wound dressings such as bandages, gauze, and cotton wool have severe adhesion to tissue proteins when applied to wounds. This may cause secondary injury to the new tissue and granulation tissue in the affected part when the dressing is replaced, resulting in pain and discomfort for the patient.[2] Moreover, traditional dressing is not conducive to wound recovery due to the lack of air permeability and moisture retention. In order to improve the shortcomings of traditional dressing, several methods for fabricating new dressings, including permeable films, foams, hydrogels, and nanofibers, have been developed.[3] Among them, the nanofibers fabricated by electrospinning technique have received extensive attention by virtue of their high specific surface area, numerous interconnected pores, good air permeability, and water absorption, as well as the ability to mimic natural extracellular matrix, making them applicable to wound dressings.[4−6] Current research studies are mainly focused on using natural polymers, e.g., chitosan, cellulose, and alginate, as well as synthetic polymers, e.g., polyurethane (PU), poly(ethylene oxide) (PEO), poly(lactic acid) (PLA), and poly(ε-caprolactone) (PCL), to fabricate electrospun nanofibers for wound dressings.[3,7,8] Despite the advantages of nanofibers, most polymeric materials for the preparation of nanofibers are susceptible to undesirable biofouling, which might cause severe wound adhesion and microbial proliferation, further hindering normal cell proliferation and greatly delay wound healing.[9] In addition, biofouling adhesion will cause a cascade of biological responses. Protein adsorption onto the material surface is the initial stage, which induces the neutrophil rapid infiltration and discharge of soluble factors such as cytokines, chemokines, reactive oxygen species (ROS), and other enzymes. In the next

Received: June 5, 2023
Accepted: September 15, 2023
Published: September 28, 2023

stage, macrophages and undifferentiated monocytes are recruited to the wound site, resulting in the inflammatory response and the formation of granulation tissue within the dressing.[10] This response not only impedes their function of dressings and delays the wound healing, but also the newly formed tissue is traumatized and causes pain in the patients during the dressing changes. Therefore, antifouling adhesion properties are demanded for wound dressings. Zwitterionic polymers are considered ideal biomaterials because of their excellent superhydrophilicity and distinguished ultralow biofouling properties.[11−13] They have an equal amount of positively and negatively charged moieties on a polymer unit, resulting in a net charge of zero. This characteristic enables them to effectively interact with water molecules through ionic solvation. The formation of a surface hydration layer serves as a physical and energetic barrier to inhibit the attachment of proteins, microbes, and cells to the surface of polymers. Therefore, zwitterionic polymers are promising for use as nonadherent wound dressing materials, which may avoid harm to healing tissue and can be effortlessly removed without causing discomfort to patients. Among the variety of zwitterionic polymers, poly(2-methacryloyloxyethyl phosphorylcholine) (PMPC) has attracted great attention because of its good biocompatibility as well as excellent resistance to nonspecific protein and biomolecule adsorption.

Another challenge for current electrospun wound dressings is their lack of antibacterial ability, and it is difficult to satisfy the requirement for long-lasting antibacterial properties during the use of wound dressing. Incorporating antimicrobial agents such as antibiotics into dressings is the conventional approach utilized to treat bacterial infections. Zhao et al. fabricated nanocarrier-embedded nanofibrous membranes loaded with tetracycline hydrochloride (TCH) using the coelectrospinning and photo-cross-linking methods and evaluated them both in vitro and in vivo to prove the long-lasting antibacterial infection.[13] The overuse of antibiotics, however, causes the emergence of antibiotic-resistant bacteria, which significantly diminish their efficacy and threaten human health. Recently, antibacterial photodynamic therapy (aPDT) has emerged as an alternative approach for cancer treatment and infectious diseases.[14−16] It relies on the production of highly cytotoxic ROS, such as singlet oxygen ($^1O_2$), by appropriately light-activated photosensitizers (PS) in the presence of molecular oxygen, which can effectively kill pathogenic bacteria without inducing the emergence of undesirable drug-resistant strains.[14,17,18] In addition, the short lifetime (microseconds to milliseconds) and limited diffusion pathway (only tens to hundreds of nanometers) of singlet oxygen in aqueous environments allow it to quickly convert into a bioharmless substance without interfering with surrounding proliferating cells and deeper tissues.[19] Incorporating the PS on a nanostructure or carrier not only facilitates an increase in the local concentration of PS and more efficient generation of toxic $^1O_2$ but also assists in obtaining tolerance to repeated treatments. Currently, aPDT in combination with nanofibers has received a great attention. Jedelská et al. prepared an indocyanine green (ICG)-loaded poly(D,L-lactide) nanofibrous mat as an aPDT wound dressing. The nanofibrous mat demonstrated prolonged resistance to hydrolysis under various pH conditions and exhibited good biocompatibility. The bacterial viability against *Staphylococcus saprophyticus*, *Escherichia coli* (*E. coli*), and *Staphylococcus aureus* (*S. aureus*) was significantly reduced by more than 99% upon laser irradiation.[20] El-Kemary et al. fabricated a cellulose acetate (CA)-based electrospun nanofiber incorporated with methylene blue (MB) for antimicrobial photoactivity against bacteria as well as an aligned CA-based trilayered nanofiber loaded with ciprofloxacin (Cipro) by the layer-by-layer electrospinning technique, which was both used as drug delivery dressings for chronic wound healing. They applied nanofibers loaded with MB followed by Cipro-loaded ones to the same wound of a mouse to achieve a combination therapy of aPDT and antibiotics. The results showed that a combination therapy was significantly superior to monotherapies, as evidenced by the enhancement in re-epithelization, collagen deposition, CD34 and TGF-$\beta$ expression, as well as a decrease in CD95+ cells.[21] Although these electrospun nanofibers combined with aPDT have demonstrated excellent antimicrobial photoactivity against bacteria, the biofouling-resistant ability and long-lasting antibacterial infection during wound healing have not yet been explored. The long-lasting antibacterial activity is beneficial for reducing dressing change frequency and helping prevent continuing drug-resistant strain development. Our previous study has developed zwitterionic core−sheath nanofibers containing MB in either shell or core layer via coaxial electrospinning technology, which showed not only good aPDT against *S. aureus* and *E. coli* but also prominent in vitro biocompatibility and antifouling performance. However, this study had an insufficient evaluation on the long-lasting aPDT effect of the nanofibers, which rendered it difficult to satisfy the requirements for long-lasting antibacterial properties during the whole wound-healing process. Herein, we integrated the advantages of fabric characteristics of electrospun nanofibers, antifouling performance of the zwitterionic polymer, and aPDT to develop a sustained antibacterial PDT wound dressing through electrostatic attraction between the positively charged photosensitizer and the zwitterionic moiety. The photosensitizer, MB, was chosen to perform aPDT because of its high triplet quantum yield ($\Phi_T \approx 0.52$), long excitation wavelength, good water solubility, low cost, and reported photodynamic inactivation against several Gram-positive and Gram-negative bacteria.[22−24] However, the hydrophilic and ionized characteristics of MB cause rapid release in the initial period, which makes it difficult to satisfy the demand for long-lasting antibacterial requirements. To meet the requirement and avoid using nanocarriers or tedious chemical modification of MB or polymer, we proposed a facile approach by means of the electrostatic interaction between MB and the zwitterionic moiety. We expected that it can avoid the burst release at the initial period and achieve the sustained release of drugs that further endows the nanofibrous mat with a long-lasting antibacterial effect. Physicochemical properties of zwitterionic nanofibrous mats, such as wound dressings, antifouling characteristics, cytocompatibility, sustained drug release profile, and long-lasting singlet oxygen production, were systematically evaluated. Antibacterial photodynamic activity was assessed against Gram-positive *S. aureus* and Gram-negative *E. coli* to verify the long-lasting antibacterial activity of the zwitterionic nanofibers.

## 2. EXPERIMENTAL SECTION

**2.1. Materials.** Bovine serum albumin (BSA, Sigma-Aldrich), bicinchoninic acid (BCA) protein assay kit (Thermo Fisher Scientific), calcium hydride (Alfa Aesar), 2′,7′-dichlorodihydro-fluorescein diacetate (DCFH-DA, Thermo), MB (Sigma-Aldrich), MPC (Sigma-Aldrich), sodium dodecyl


https://doi.org/10.1021/acsomega.3c03964
ACS Omega 2023, 8, 36906−36918

sulfate (SDS, Riedel-deHaen), and stannous octoate (Sigma-Aldrich) were used as received. Common organic solvents were obtained commercially from Sigma-Aldrich, ECHO, J. T. Baker, or Macron and used as received. Singlet oxygen sensor green (SOSG, Life Technologies) was performed according to the manufacturer instruction. Azobis(isobutyronitrile) (AIBN) (Aencore, 99%) was recrystallized from ethanol. ε-Caprolactone (Alfa Aesar, 99%) was distilled over $CaH_2$ under reduced pressure. 2-Hydroxyethyl methacrylate (HEMA, Acros, 97%) was purified by multistep extraction from *n*-hexane, followed by diethyl ether. 3-(4,5-Dimethyl-2-thiazolyl)-2,5-diphenyl-2*H*-tetrazolium bromide (MTT) was obtained from Bionovas. Antibiotic−antimycotic solution (100×), Dulbecco's phosphate-buffered saline (DPBS 1×), fetal bovine serum (FBS), Minimum Essential Medium (MEM 1×), and trypsin−EDTA (1×) were purchased from Corning and used as received. Müller−Hinton agar (MHA), tryptone soy agar (TSA), and tryptone soy broth (TSB) were purchased from Becton Dickinson. 2-Benxyl 2-hydroxyethyl carbonotrithioate (BHECT) was synthesized according to the published literature.[25]

**2.2. Synthesis of Macroinitiator PCL-CTA.** Initiator BHECT (0.1 g, 0.5 mmol) was placed in a round-bottomed flask with a stir bar and vacuumed for 1 h. Under a nitrogen atmosphere, ε-caprolactone (23.4 g, 205 mmol) and stannous octoate (65 mg, 0.16 mmol) used as catalysts were added into the flask. The reaction mixture was placed in a preheated oil bath at 120 °C for 20 h. Then, a certain amount of THF was added to the resulting viscous solution and purified by precipitation into cold methanol three times. Finally, the product was dried in a vacuum oven to obtain PCL-CTA (PCL) as a light yellow solid (15 g, 63%). $M_{n(NMR)}$ = 39,494, DP = 343, $M_{n(GPC)}$ = 25,800, $M_{w(GPC)}$ = 41,700, and PDI = 1.62.

**2.3. Synthesis of PCL-*b*-PMPC and PCL-*b*-PHEMA.** Both block copolymers were synthesized using the reversible addition−fragmentation polymerization method. Typically for the synthesis of PCL-*b*-PMPC, the PCL-CTA macroinitiator (2.0 g, 0.05 mmol) was added into a Schlenk tube and then vacuumed for 1 h, followed by a nitrogen backfill. A solution of MPC (1.5 g, 5 mmol) and AIBN (1.7 mg, 0.01 mmol) in a cosolvent of DMSO/MeOH (10 mL, 4:1, v/v) was added into the Schlenk tube after nitrogen was bubbled through the solution for 30 min. The mixture was degassed three times using a freeze−pump−thaw process and then backfilled with $N_2$. Then, the Schlenk tube was immersed in an oil bath at 85 °C for 20 h. After polymerization, the reaction mixture was transferred into a dialysis membrane (Cellu Sep, MWCO 12,000−14,000 Da) against a mixture solvent of THF/MeOH (1:1, v/v) for 24 h to remove solvent or unreacted reactants. The dialysis medium was replaced every 12 h. Finally, the solution was concentrated and then precipitated in diethyl ether to obtain 2.7 g of PCL-*b*-PMPC (PM) copolymer with light yellow color. PCL-*b*-PHEMA (PH) was synthesized with the same procedure but replacing the MPC monomer with the HEMA monomer (0.7 g, 5 mmol) and the mixture solvent with DMSO (10 mL). The PH copolymers were lyophilized to obtain 2.1 g light yellow powders. PCL-*b*-PHEMA: $M_{n(NMR)}$ = 52,154, $DP_{HEMA}$ = 97, $DP_{PCL}$ = 343; PCL-*b*-PMPC: $M_{n(NMR)}$ = 65,679, $DP_{MPC}$ = 85, and $DP_{PCL}$ = 343.

**2.4. Fabrication of Electrospun Nanofibrous Mats.** PCL-CTA, PCL-*b*-PHEMA, and PCL-*b*-PMPC copolymers with or without loading of a photosensitizer, MB (3 wt % corresponding to copolymer) were dissolved in a $CHCl_3$/MeOH (2:1, v/v) solvent mixture with polymer concentration of 40% for PCL-CTA and PCL-*b*-PHEMA and 23% for PCL-*b*-PMPC. The solutions were magnetic-stirred at room temperature for 12 h. The ES nanofibers were fabricated using a single-capillary spinneret. The corresponding solution was fed into a 22-gauge metallic needle using a syringe pump (Fusion 100, Chemyx Inc.) at a flow rate of 0.3 mL $h^{-1}$. The metallic needle was connected to a high-voltage supply (You-Shang Technical Corp.) with an applied voltage of 15 kV for plain nanofibers and 20 kV for MB-loaded nanofibrous mats. The nanofibers were collected onto a piece of aluminum foil placed 15 cm below the tip of the needle for 2 h. All experiments were performed at room temperature and around 30% relative humidity. The plain nanofibrous mats were assigned **PCL**, **PH**, and **PM**, as well as MB-loaded nanofibrous mats were assigned **PCL-MB**, **PH-MB**, and **PM-MB**.

**2.5. General Characterization.** $^1$H NMR spectra were measured in $CDCl_3$, DMSO-$d_6$, and $CDCl_3$/$CD_3OD$ (2:1, v/v) for PCL-CTA, PCL-*b*-PHEMA, and PCL-*b*-PMPC, respectively, by a Bruker-DPX-400 instrument spectrometer (Bruker, Rheinstetten, Germany) operating at 400 MHz. The morphologies of the ES nanofibers were characterized by field-emission scanning electron microscope (FE-SEM, Hitachi S4800). The samples cut into 5 × 5 mm were vacuum-dried at 50 °C for 24 h and then sputtered with a coating of platinum for 30 s before measurement. SEM images from each sample were analyzed to obtain the average diameter of over 50 nanofibers. The aqueous stability of the nanofibers was evaluated by immersing the samples into deionized water for 24 h, followed by lyophilization of the samples for SEM observation. Static water contact angles were determined using a contact angle goniometer (CAM-100, Creating Nano Technologies Inc.). About 5 μL of water droplet was deposited onto a nanofibrous mat (1 cm × 1 cm), which was mounted onto a glass slide. At 0, 10, 30, and 50 s, photographs of the water/nanofiber interface were recorded. The photosensitizer (MB) loaded content was examined by UV−visible spectroscopy (UV2600, Shimadzu) with reference to a calibration curve of MB in $CHCl_3$/MeOH (2:1, v/v). The MB loading efficiency (LE) was calculated from the weight ratio of MB loaded in nanofibers to the total MB fed. Each MB-loaded nanofibrous mat was repeated in triplicate to determine LE.

**2.6. Measurement of Water Absorption Ability, Water Retention Capability, and Water Vapor Permeability.** The water absorption ability of the ES nanofibrous mats (**PCL**, **PH**, and **PM**) was gravimetrically determined by the direct water-immersed method and contact sponge test that simulated contact on the wound. The completely dried nanofibers were weighed ($W_d$), followed by immersion in either deionized water or placing them onto a water-soaked sponge at room temperature. At predetermined time intervals, the wet samples were weighed ($W_s$) immediately after gently wiping with Kimwipes. Each condition of various nanofibrous mats was performed in triplicate. The water absorption ratio of the nanofibers was determined according to the following equation

$$\text{water absorption } (W_A\ \%) = \frac{W_s - W_d}{W_d} \times 100\%$$

Water retention capability was determined by maintaining wet nanofibrous mats (immersed in deionized water for 24 h)


https://doi.org/10.1021/acsomega.3c03964
ACS Omega 2023, 8, 36906−36918

at 25 °C and 45 ± 5% relative humidity for different time periods. The dried nanofibers ($W_d$) and wet nanofibers ($W_s$) were weighed before testing. At specific time intervals (time $t$), the samples were weighed ($W_t$) to calculate the water retention capability as follows, and three measurements were conducted

$$\text{water retention } (W_R\ \%) = \frac{W_t - W_d}{W_s - W_d} \times 100\%$$

The water vapor permeability (WVP) was assessed according to the modified reported method to evaluate the moisture permeability of the nanofibrous mats.[26] The nanofibrous mat was cut into a disc (1 $cm^2$) with a thickness of around 0.125 ± 0.005 mm and fixed on the mouth of a glass vial containing deionized water (3 mL). A glass vial without a cover of any nanofiber was used as a control group. The sample was put into a chamber maintained at 25 °C and 50% relative humidity for 48 h. Then, the watering-containing vials at an initial time and after 48 h were weighted. Each condition was conducted in triplicate. The WVP was calculated using the following equation

$$\text{WVP} = \left(\frac{\Delta W}{A \times \Delta t}\right)$$

where $\Delta W$ is the weight change due to water vapor permeation (g), $A$ is the area of exposed film ($m^2$), and $\Delta t$ is the change in time (d).

**2.7. Assessment of Protein Adsorption and Cell Adhesion.** The quantitative assessment of protein adsorption on the nanofibrous mats was investigated according to the reported method.[27,28] Briefly, the nanofibrous mat of 1 × 1 $cm^2$ dimensions was immersed in PBS buffer for 24 h and transferred into 1 mL of fresh BSA solution (2 mg $mL^{-1}$) at 37 °C for 3 h. Then, the mats were put into 0.1 wt % SDS solution and ultrasonicated for 10 min to remove unadsorbed protein. Afterward, the adsorbed proteins were desorbed by placing the resulting nanofibrous mats into 1 mL of 3 wt % SDS solution and ultrasonicated for 30 min at 37 °C. The protein sample was added to the BCA working reagent with a sample to working reagent ratio of 1:8 (v/v), followed by incubation at 37 °C for 30 min. The adsorbed BSA concentration was evaluated by the absorbance at 562 nm using a microplate reader (BioTek-MQX200, Agilent) and then calculated with a calibration curve prepared by mixing BSA protein with the BCA reagent at different concentrations. Each sample was measured in triplicate. For the qualitative evaluation of protein adsorption on the nanofibers, briefly, the mat of 1 × 1 $cm^2$ dimensions was placed into the BSA-FITC solution (1 mg $mL^{-1}$) at 37 °C for 4 h. After removal of the mat and rinsing with PBS, the mat was mounted on a slide and examined using a confocal laser scanning microscope (CLSM, Olympus FV 1000). PCL and PH nanofibrous mats were used as the control groups.

The nanofibrous mats were sterilized with 75% ethanol, followed by rinsing with sterile DPBS thrice, and then put onto the coverslip and placed into a 24-well plate individually. The mouse fibroblast cell line (L929 fibroblast cells) was seeded at a density of 5 × $10^4$ cells/well and cultured in an MEM supplemented with 10% FBS and 1% of antibiotics (penicillin–streptomycin solution). After incubating at 37 °C in a 5% $CO_2$ atmosphere for 24 h, the mat was washed two times with DPBS and stained with a cell-permeant DNA dye, Syto-9 (5 μM, 15 min). After washing with PBS, the samples were fixed on a slide for fluorescent signal detection by CLSM with an excitation wavelength of 488 nm for Syto-9.

**2.8. In Vitro Drug Release Behavior.** MB-loaded nanofibrous mats (**PCL-MB**, **PH-MB**, and **PM-MB**) were immersed in 20 mL of deionized water at 37 °C. At specific time intervals, 3 mL of solution was collected and replaced with an equal volume of fresh deionized water. The amount of MB released was determined by UV–visible spectroscopy (Shimadzu UV-2450 spectrophotometer). Each sample was analyzed in triplicate. After 720 min, the resulting nanofibers were lyophilized and redissolved in 1 mL of $CHCl_3$/MeOH (2:1, v/v). The amount of the MB residue was also calculated by absorbance measurements.

**2.9. ROS Production Measurement.** The production of ROS was monitored using a SOSG reagent according to the manufacturing protocol. The MB-loaded nanofibrous mats (**PCL-MB**, **PH-MB**, and **PM-MB**) containing 25.3 ± 3.2 μg MB were mounted on a glass slide and put into a sample vial containing 10 mL of the SOSG solution (5 μM in an oxygen-saturated deuterated water). Then, the corresponding sample solution was irradiated under a halogen lamp (50 W $m^{-2}$) equipped with a filter passing only 525–800 nm light for different periods of time. 3 mL of the solution was taken into a cuvette, and the oxidized SOSG was quantified by recording the fluorescent intensity at 530 nm with an excitation wavelength of 488 nm (Hitachi F-7000 spectrometer). Plain nanofibrous mats and free MB were examined with the same procedure. All of the experiments were performed at room temperature in the dark.

**2.10. Cytotoxicity Testing.** To evaluate the biocompatibility of the plain and MB-loaded nanofibrous mats, a mouse fibroblast cell line (L929) was selected to conduct the MTT assay. L929 cells were seeded in 24-well plates at a density of 5 × $10^4$ cells per well and incubated at 37 °C in a 5% $CO_2$ atmosphere for 24 h. Then, sterilized nanofibers (5 mm in diameter) were washed with DPBS and carefully placed in each well by adding 2 mL of fresh medium. The amount of MB in nanofibrous mats was fixed around 23.7 ± 0.6 μg. The cytocompatibility and phototoxicity were conducted in the dark or under irradiation using a halogen lamp (equipped with a filter passing only 525–800 nm light) at a power density of 50 or 100 W $m^{-2}$ for 60 min. All the culture plates were incubated for another 24 h under the standard cell culture condition. Then, the cell viability was evaluated by the MTT assay after the removal of the nanofibers. Each sample was performed in triplicate. Cells were seeded on the tissue culture plate (TCP) without any treatment as a control group.

**2.11. Antibacterial Photodynamic Therapy Assay.** Gram-positive *S. aureus* (ATCC 25923) and Gram-negative *E. coli* (DH5α) were chosen as the model strains. The disc diffusion method was employed to evaluate the aPDT performance of the nanofibers by determining the inhibition zone (halo width) in the dark or under irradiation. The bacterial suspension was appropriately diluted in TSB to achieve a density of 1.5 × $10^8$ CFU per milliliter. All broth and nanofibrous mats used in this study were sterilized. Briefly, 100 μL of an *E. coli* or *S. aureus* suspension was uniformly spread on MHA plates. Samples of nanofibrous mats (5 mm in diameter) were placed onto the respective agar plates and then incubated in the dark at 37 °C for 24 h as a control group or irradiated with a halogen lamp (equipped with a filter passing only 525–800 nm light) at a power density of 50 or 100 W $m^{-2}$ for 60 min. Subsequently, the samples were incubated in


https://doi.org/10.1021/acsomega.3c03964
ACS Omega 2023, 8, 36906–36918

**Scheme 1. Schematic Diagram for Fabrication of an Antibiofouling Nanofibrous Mat with Long-Lasting Antibacterial Photodynamic Therapy**

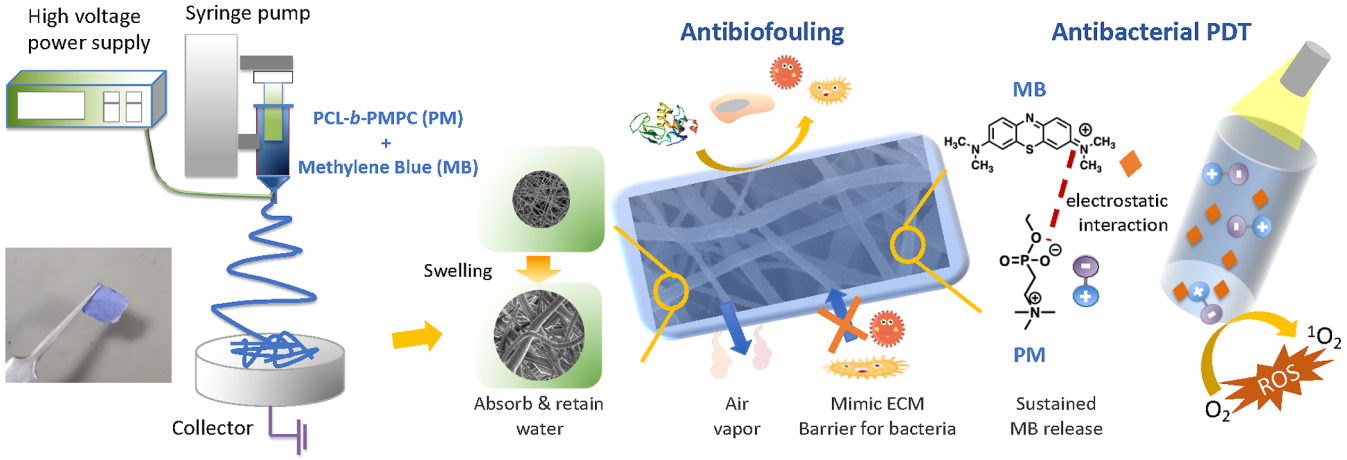


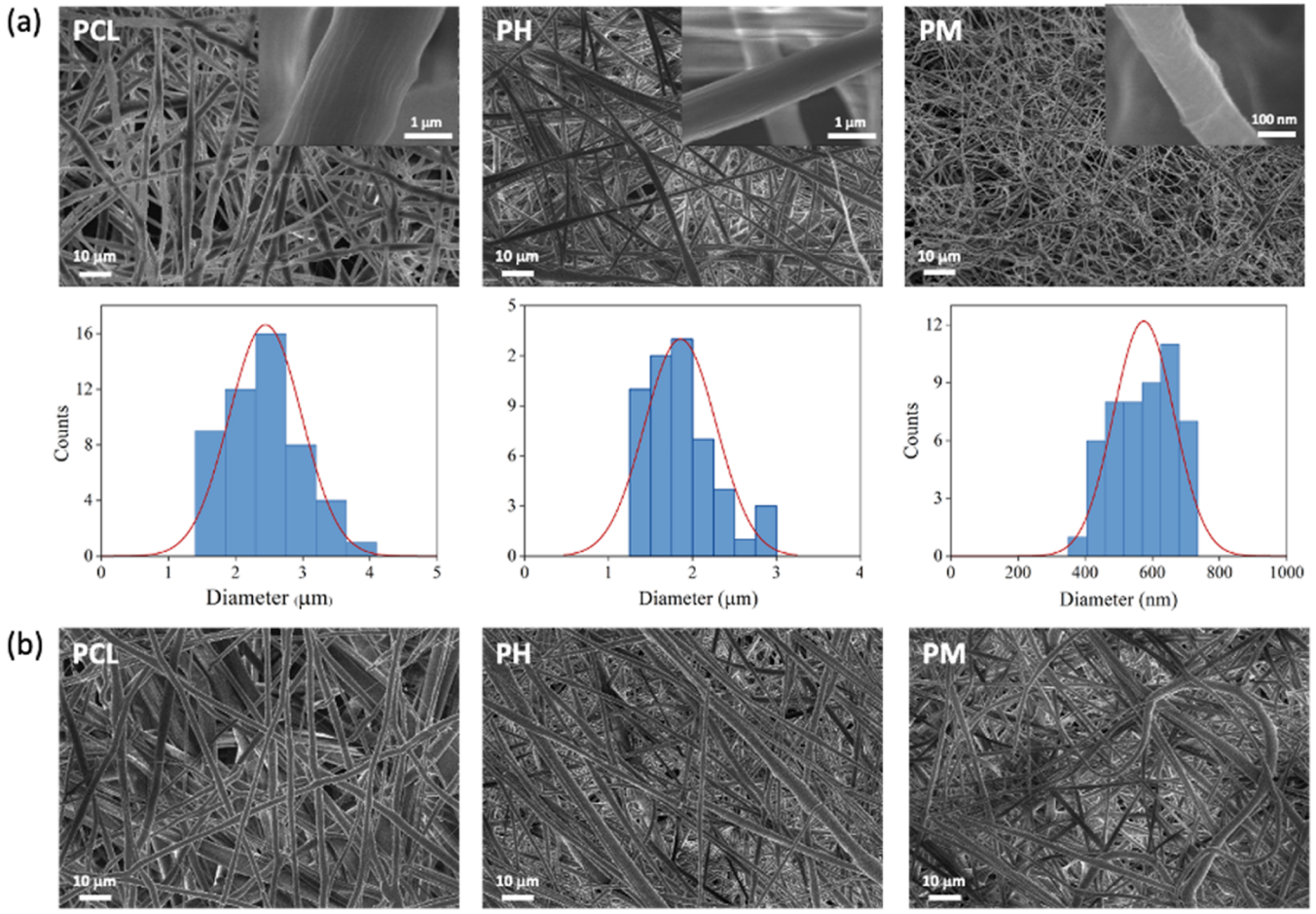


**Figure 1.** (a) FE-SEM images and its diameter distribution of various nanofibrous mats (**PCL**, **PH**, and **PM**); (b) FE-SEM images of various nanofibrous mats after being immersed in aqueous media at room temperature for 24 h.

the dark at 37 °C for an additional 24 h. The amount of MB in the nanofibers was fixed at around 23.7 ± 0.6 μg. The inhibition halo diameter was determined by the clear zone in the absence of bacterial growth detected by the naked eye. Antibiotics such as tetracycline and kanamycin (25 μg) dissolved in aqueous solution were dropped on the disc (5 mm in diameter) and then lyophilized. The antibacterial experimental procedure was the same as that of the nanofibrous mats but without illumination. All experiments were performed in triplicate under each condition.

## 3. RESULTS AND DISCUSSION

**3.1. Preparation and Characterization of Electrospun Nanofibrous Dressing.** The objective of the present study was to prepare a zwitterionic nanofibrous mat loaded with PS capable of both the antibiofouling capabilities and the



https://doi.org/10.1021/acsomega.3c03964
ACS Omega 2023, 8, 36906−36918

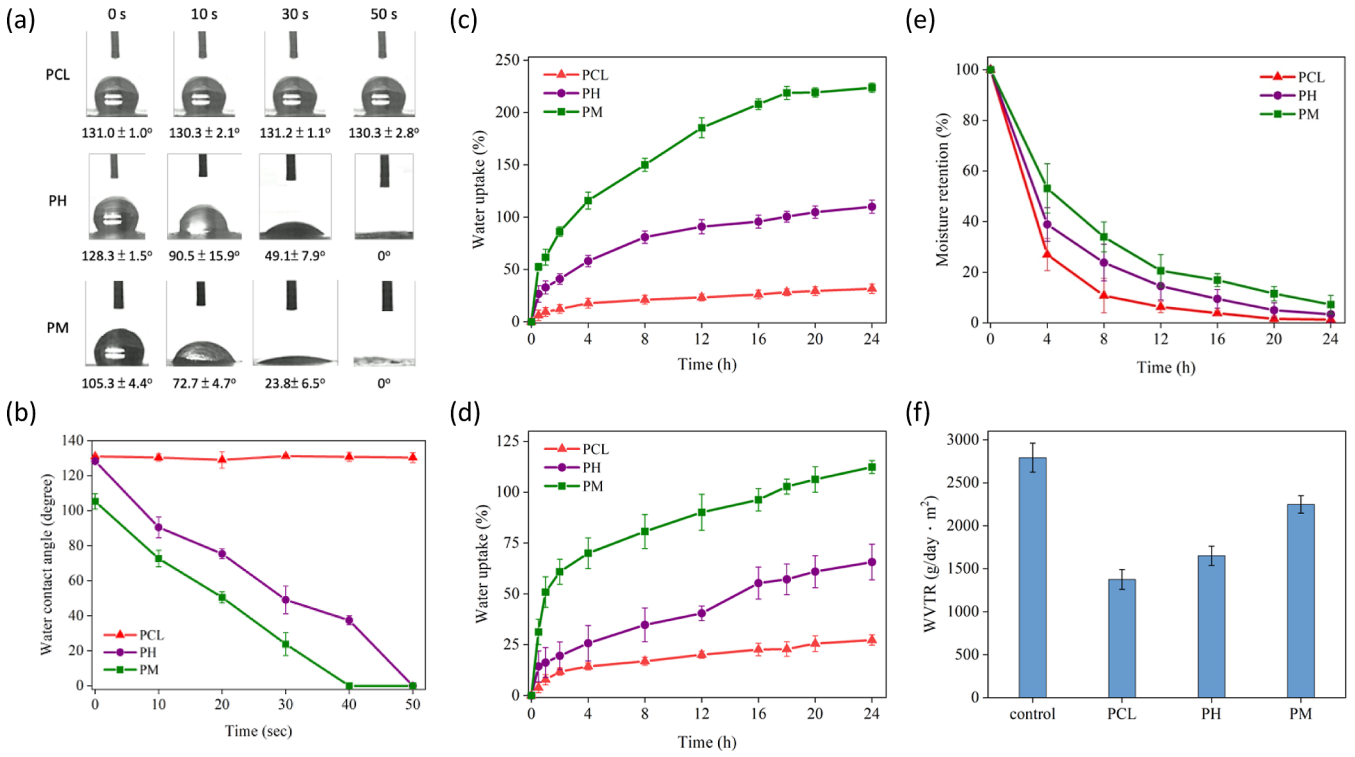


**Figure 2.** Physicochemical characterization of **PCL**, **PH**, and **PM** nanofibers: (a) digital photos of water contact angle (WCA) from the corresponding nanofibers within 50 s; (b) WCA as a function of time for different nanofibers; water absorption ability via (c) direct water immersed method and (d) contact sponge test; (e) water retention capability; and (f) water vapor permeability.

sustained release of photosensitizer for aPDT, as illustrated in Scheme 1. This was achieved through electrospinning of the block copolymer (PCL-*b*-PMPC) containing the zwitterionic poly(2-MPC) and biocompatible poly(*ε*-caprolactone) (PCL), where the zwitterionic polymers have been demonstrated possessing ultralow biofouling characteristics as a result of the creation of a hydration layer on the surface of biomaterials.[11,29] The biocompatible PCL and the first generation of antifouling materials, poly(2-hydroxyethyl methacrylate) (PCL-*b*-PHEMA), were also prepared using the same technique as counterparts for comparison of their antibiofouling, antibacterial, and wound dressing properties. The synthetic routes of these polymers (PCL, PCL-*b*-PHEMA, and PCL-*b*-PMPC) via ring open polymerization and reversible addition−fragmentation chain transfer were as illustrated in Scheme S1 (Supporting Information). The compositions and chemical structures of these series of polymers were characterized by $^{1}$H NMR spectra (Figure S1 in the Supporting Information).

*3.1.1. Morphological Investigation.* The optimization of electrospinning parameters and polymer/photosensitizer ratio for the fabrication of plain nanofibers (namely, **PCL**, **PH**, and **PM**) was thoroughly investigated. Figure 1a shows the FE-SEM images of various electrospun nanofibers, which exhibited a bead-free and smooth surface with random orientation and almost uniform diameters throughout their lengths. The average diameters of **PCL**, **PH**, and **PM** nanofibers were 2.45 ± 0.54 $\mu$m, 1.86 ± 0.43 $\mu$m, and 574 ± 90 nm, respectively, which were calculated over 50 nanofibers by ImageJ. It is known that insufficient polymer concentration is not conducive to fiber formation due to a lack of sufficient concentration for chain entanglement.[30] Molecular weight and concentration are decisive factors.[30] The lower the molecular weight, the smaller the entanglement content, which needs to be compensated by increasing the concentration, but this causes an increase in the average diameter of the fiber. The lower polymer concentration and small fiber diameter of **PM** nanofibers compared to **PCL** and **PH** used to fabricate nanofibers might be attributed to the presence of electrostatic interaction between zwitterionic groups of PCL-*b*-PMPC. It increases the electrical conductivity of the polyelectrolyte solution, facilitating the smooth formation of uniform and finer nanofibers.[31,32] The aqueous stability of different nanofibers was examined by immersing them in an aqueous environment at room temperature for 24 h, followed by vacuum-drying for the SEM measurement. Figure 1b shows that all of the nanofibers preserved their fibrous shape in water, suggesting that they had good aqueous stability. The average diameters of **PCL**, **PH**, and **PM** nanofibers after immersion were 2.46 ± 0.60, 2.34 ± 0.51, and 1.84 ± 0.38 $\mu$m, respectively. No difference in the diameter of **PCL** nanofibers before and after fiber immersion in water was due to its hydrophobicity. Compared to **PH** nanofibers, the obviously swollen nanofibers of **PM** after being immersed in water were observed because of the excellent water affinity of the zwitterionic PMPC moiety, leading to higher water absorption capacity than **pH** nanofibers. This is beneficial for use as wound dressings to absorb exudates.

*3.1.2. Physicochemical Characterization.* Selecting appropriate dressings according to the type of wound is helpful for wound recovery. Traditional dressings are not conducive to wound recovery in addition to their lack of air permeability and moisture. Besides that, protein or cell adhesion leads to pain and discomfort for patients during the removal of the dressings. Since the wound dressing is directly in contact with the wound bed, the wound secretes liquid protein components to repair the damaged tissue and stop bleeding. It


https://doi.org/10.1021/acsomega.3c03964
ACS Omega 2023, 8, 36906−36918

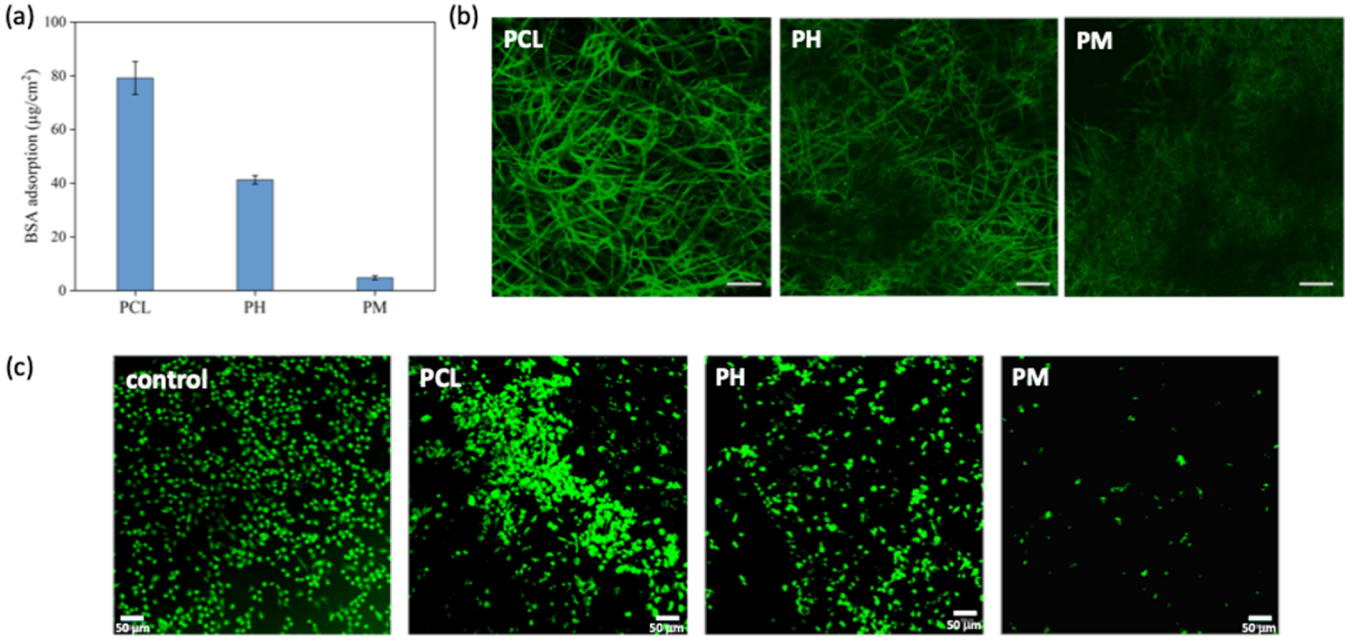


**Figure 3.** Antibiofouling evaluations of **PCL**, **PH**, and **PM** nanofibers: (a) BSA protein adsorption on the surfaces of nanofibers; (b) CLSM images of BSA-FITC adhered on nanofibers (scale bar is 40 $\mu$m); and (c) CLSM images of L929 cells adhered on nanofibers (scale bar is 50 $\mu$m).

is very important for dressings to have antibiofouling adhesion properties and to be easily removed or replaced to reduce damage to new wound tissue in clinical wound healing.[28] The ideal wound dressing should adsorb excess wound exudates, maintain moderate moisture in the wound bed, provide good oxygen permeability, and resist protein or cell adhesion and noncytotoxicity. Therefore, the physicochemical characterization of the as-prepared nanofibrous mats, including hydrophilicity, exudate adsorption capability, and WVP was assessed.

The surface hydrophilic properties of the **PCL**, **PH**, and **PM** nanofibers were performed by water contact angle measurement (Figure 2a,b). The hydrophilic nature of PHEMA and PMPC segments caused **PH** and **PM** nanofibers to possess high wettability and minimal contact angle of zero within 50 s, while **PCL** nanofibers maintained a contact angle of approximately 130.3 ± 2.8°. Furthermore, the contact angle decreases over time because of the distribution of hydrophilic segments on the **PH** and **PM** fibrous surfaces, resulting in water droplets being absorbed into the fiber through capillary action. The faster decrease in the contact angle of **PM** than **PH** nanofibers was speculated as the strong interaction with water via electrostatic forces induced by the zwitterionic structure of PMPC. Since the energy of the electrostatic force is higher than that of the hydrogen bond between OH group and the water molecule resulting from PHEMA,[28] the water absorption rate of **PM** nanofibers was enhanced.

During wound formation, a large amount of interstitial fluid is secreted to resist the invasion of foreign microorganisms and repair the wound. Excessive wound exudates tend to cause maceration of the wound and microbial propagation, which delays wound healing.[33,34] However, excessive dryness of the wound is unfavorable for wound healing and may cause scars after recovery.[35] Therefore, a dressing with appropriate water absorption ($W_A$) and water retention capability ($W_R$) is conducive to controlling exudates and regulating the wound moisture balance. The water absorption capacity of **PCL**, **PH**, and **PM** nanofibrous mats was analyzed by the direct water immersed method and contact sponge test. As presented in Figure 2c,d, **PM** had the best water absorption capability as compared to **PH** and **PCL** mats, regardless of whether the nanofibrous mats were directly immersed in water or used the sponge method to simulate the wound. The lower water absorption ability for the **PCL** mat was due to their hydrophobic property. The water absorption ability of **PM** and **PH** mats was through electrostatic forces between the zwitterionic moiety and water molecules or hydrogen bond forces between hydroxyl (OH) groups and water molecules, respectively. The water absorption ratio of the **PM** nanofibrous mat was around twofold higher than that of the **PH** mat, which might be due to the stronger electrostatic force than the hydrogen bond with water molecules.[28] In addition, the smaller diameter of the **PM** nanofibers provided more voids to accommodate water molecules. This result indicated that the high hydrophilicity of zwitterionic PMPC can improve the water penetration to the nanofibers and increase its water absorption and hydration ability. The fast increase in water absorption of the **PM** mat within the initial hour indicated its effective absorption capacity to eliminate exudate. Figure 2e shows that the water retention of **PCL**, **PH**, and **PM** mats is 4.83 ± 2.6, 11.74 ± 5.45, and 20.78 ± 7.84% after 24 h, respectively. The hydrophobic nature of the **PCL** mat caused the limited water absorption capability and difficulty in maintaining the moisture. The hydrophilic properties of **PH** and **PM** mats had a strong interaction with water molecules that not only facilitated water absorption but also reduced water evaporation and maintained the moisture content of the wound. Likewise, the **PM** nanofibrous mat had a better moisturizing effect than the **PH** mat. The proper WVP is also important to adjust the wound moisture balance. An ideal WVP should be in the range of 2000−2500 g $day^{-1}$ $m^{-2}$ without leading to the accumulation of wound exudate to infiltrate the wound or bacteria breeding[34] and the dehydration of the wound excessively. From the results, the WVP values of


https://doi.org/10.1021/acsomega.3c03964
ACS Omega 2023, 8, 36906−36918

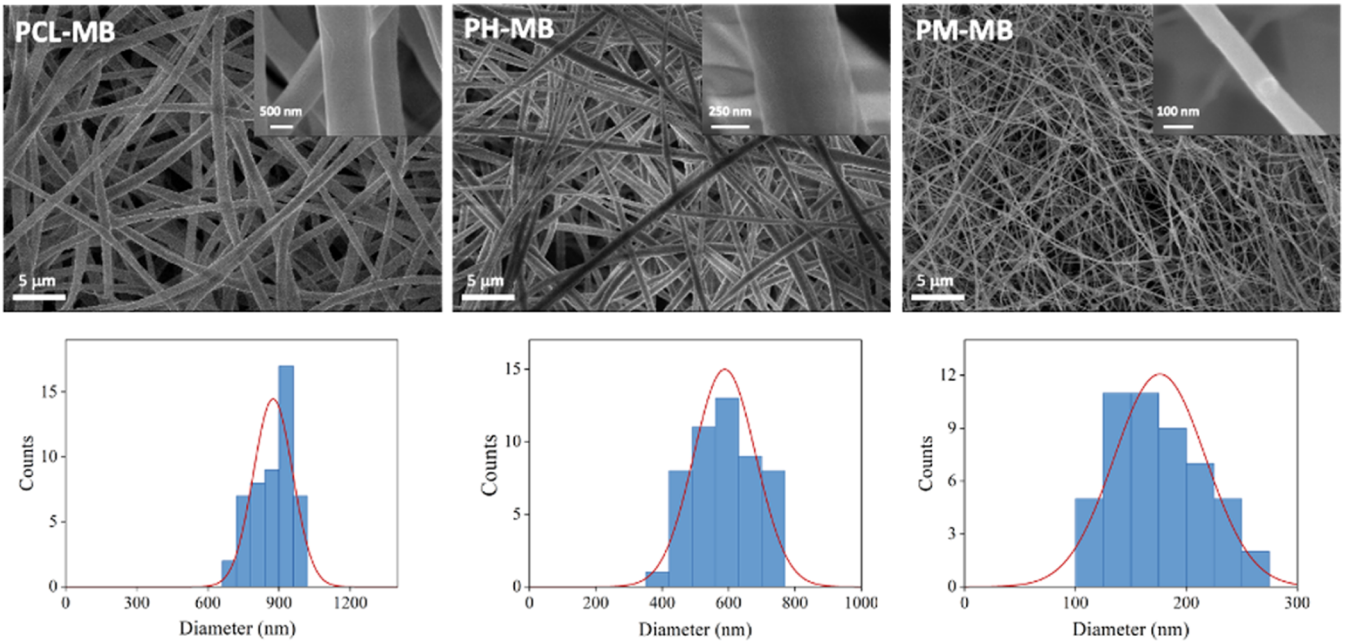


**Figure 4.** FE-SEM images and their diameter distribution of various MB-loaded nanofibers (**PCL-MB**, **PH-MB**, and **PM-MB**).

all nanofibrous mats were lower than that of the control group (without cover of any nanofibers) (Figure 2f), indicating that all of the mats had the ability to prevent evaporation of wound fluids. On the other hand, the WVP value relies on the diffusivity of water, which is influenced by the interaction between nanofibers and water molecules. The **PCL** mat showed the lowest WVP value because of the high hydrophobicity of **PCL** that hindered the moisture passage across the nanofibers. Interestingly, it is observed that only the WVP value of the **PM** mat fell within the ideal range. This might be attributed to high hydrophilicity and strong interaction of zwitterionic moiety with water molecules that not only allowed water to adhere onto the nanofibers and further promoted the diffusion of water through the voids to the surface but also reduced the resistance of water molecules to permeate.[36]

**3.2. Antibiofouling Performance.** Wound recovery is a series of complex biochemical reactions that will secrete a large amount of tissue fluid containing certain immune-related cells and proteins to resist the invasion of microbes and repair the damaged tissue. Since the dressing is in direct contact with the wound, the dressing is required to have high-efficiency fouling resistance properties to reduce protein and cell adhesion to the wound in clinical wound healing. In this study, the quantification of the adsorbed BSA protein was conducted by utilizing the BCA assay, and qualitative evaluation was performed using BSA-FITC by CLSM. The micro-BCA protein assay was used to assess the adsorption of BSA protein on the nanofibrous mats. As shown in Figure 3a, the **PM** mat showed that the adsorbed amount of BSA protein on the zwitterionic surface ($4.8 \pm 0.6$ $\mu g$ $cm^{-2}$) was remarkably decreased and around 16 times and 8 times less adsorbed amount of BSA protein than **PCL** ($79.2 \pm 6.1$ $\mu g$ $cm^{-2}$) and **PH** ($41.3 \pm 1.6$ $\mu g$ $cm^{-2}$) nanofibrous mats, respectively. To investigate the BSA protein adsorption qualitatively on the nanofibrous mats, various nanofibers were in contact with BSA-FITC for 3 h at 37 °C. Figure 3b shows that the hydrophobic **PCL** mat displayed bright green fluorescent signals due to the strong interaction between the PCL polymer and the hydrophobic portion of BSA proteins.[37] In contrast, the green fluorescent signals on the hydrophilic **PH** and **PM** mats were significantly reduced, especially for **PM**. According to our previous study, the strong hydration capability of zwitterionic PMPC moiety formed a thick hydration layer on the surface of nanofibers, which created a strong repulsion to inhibit surface protein adhesion and maintain the normal conformation of proteins.[38,39] In addition, zwitterionic **PM** performed stronger electrostatic interaction induction with water molecules than the hydrogen bonding generated by the OH group of **PH**, resulting in a low fouling behavior.

Fibroblast adhesion to wound dressings can delay healing, leading to an associated supplementary trauma. To investigate the resistance to cell adhesion on the nanofibrous mats, various nanofibrous mats were incubated with L929 fibroblasts for 24 h and stained with a cell-permeant nucleic acid dye, Syto-9, followed by detection using CLSM. The hydrophobic **PCL** and hydrophilic **PH** mats presented significant green fluorescence signals. The mimicry of the native extracellular matrix as well as the high area-to-volume ratio and porosity of nanofibers might serve as a proper environment for cell attachment. On the other hand, the fluorescence signal of the **PM** mat was significantly reduced due to excellent anticell adhesion properties (Figure 3c). These results were consistent with a strong hydration layer and lack of cell attachment protein owing to a zwitterionic moiety, resulting in significant resistance to cell adhesion.[40,41] Taken together with the above results, the **PM** mat providing a zwitterionic surface could efficiently inhibit the initial protein adsorption, which is recognized as a prerequisite for preventing the subsequent adhesion and proliferation of other microorganisms.[13] The advantage of the inert cell adhesion property further allows **PM** nanofibers to be used as easily removed and painless wound dressings without disturbing newly formed tissues as well as minimal scarring can be expected. Therefore, the **PM** mat can be an ideal candidate for use in nonadherent wound dressings.

**3.3. Characterization of Photosensitizer-Loaded Nanofibers.** The photosensitizer, MB, was loaded into the



https://doi.org/10.1021/acsomega.3c03964
ACS Omega 2023, 8, 36906−36918

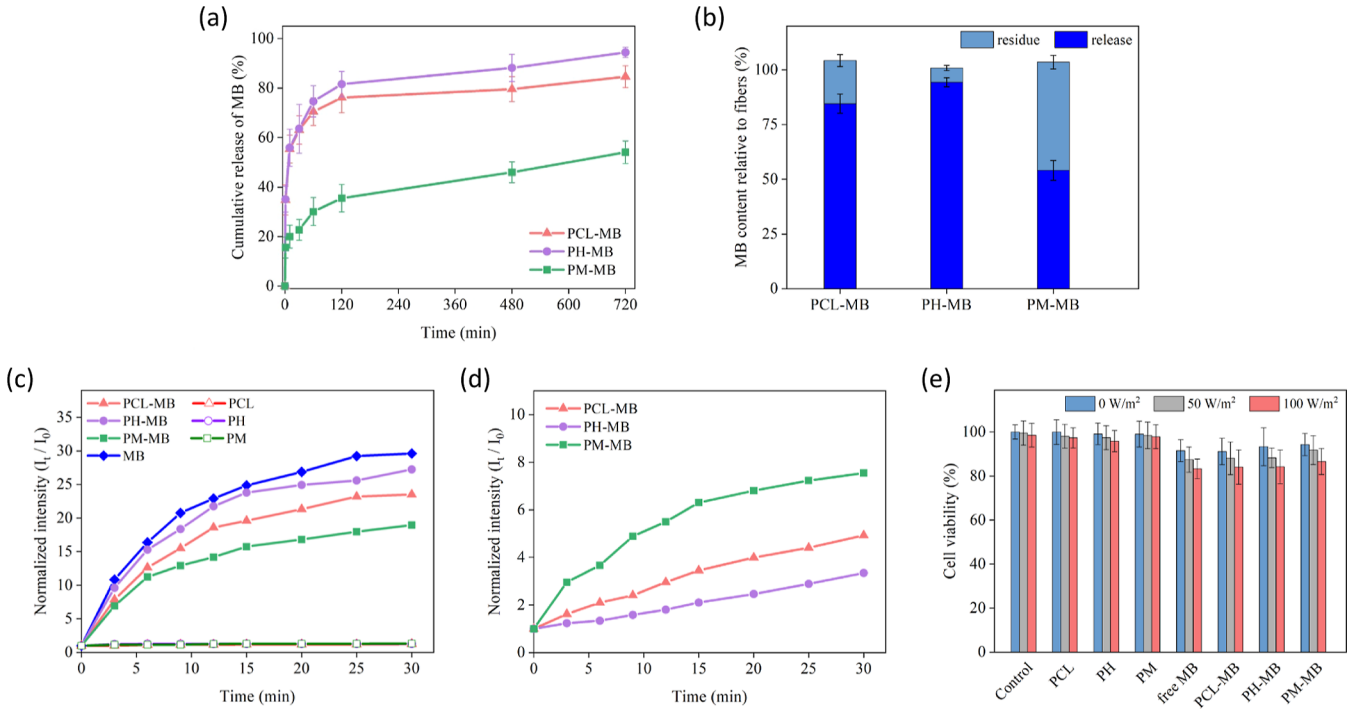


**Figure 5.** (a) In vitro MB release profiles from different nanofibrous mats; (b) histogram of MB released from and MB residual in different nanofibrous mats after MB release of 12 h; (c) singlet oxygen detection of different plain and MB-loaded mats and free MB under illumination (50 W $m^{-2}$) for various time periods using singlet oxygen sensor green as an agent; (d) singlet oxygen generation of MB-loaded nanofibrous mats after 12 h of in vitro release; (e) cell viability of L929 cells treated with plain mats, MB-loaded mats, and free MB in different illumination conditions (0, 50, and 100 W $m^{-2}$) for 60 min.

various nanofibers by electrospinning of 3 wt % of MB-added polymer solution, namely, **PCL-MB**, **PH-MB**, and **PM-MB**, respectively. The higher applied voltage (20 kV) required for fabrication of MB-loaded nanofibers than that (15 kV) for plain nanofibers suggested that the positively charged structure of MB increases the viscosity and conductivity of the solution, so applied higher voltage facilitates the polymeric jet to stretch and form the bead-free and continuous nanofibers. As presented in Figure 4, the smoother surface and smaller average diameters of the MB-loaded nanofibers compared to their corresponding plain nanofibers might be attributed to the increased operating voltage and electrostatic repulsive force due to the addition of MB. The average diameters of **PCL-MB**, **PH-MB**, and **PM-MB** were 875 ± 83, 588 ± 93, and 176 ± 41 nm, respectively, which were calculated over 50 nanofibers by ImageJ. The LE was found to be 65.7 ± 4.1% for **PCL-MB**, 76.4 ± 4.4% for **PH-MB**, and 89.3 ± 1.1% for **PM-MB**, respectively. The highest LE of **PM-MB** was observed, suggesting that the electrostatic attraction between the positively charged MB and zwitterionic PMPC moiety promoted the increase of the MB loading. This result was consistent with the literature[42] and our previously reported study.[43]

*3.3.1. In Vitro Release Behaviors and Detection of Singlet Oxygen Generation.* ROS production, mainly singlet oxygen ($^1O_2$), is the most important factor in the efficiency of aPDT. Owing to the short half-life of $^1O_2$ (about 600 ns) in the biological/cellular environment,[19] its diffusion distance is limited (about 0.1 $\mu$m) that causes the PS to be located near the target (such as bacterial cells) to provide sufficient time for generated $^1O_2$ to act on or penetrate through the cell membrane into the bacterial cells. The positively charged MB enhances the electrostatic interaction with the bacterial cell membranes, thereby enhancing its aPDT efficiency. In addition, both the efficient bacterial inhibition in the early stage of wound recovery and long-lasting antibacterial performance resulting from the sustained release capability in the later period are valuable and are demanded in clinic wound dressings. The evaluation of MB release profiles of various nanofibrous mats is presented in Figure 5a. The initial burst release within the first hour of the **PCL-MB** and **PH-MB** mats was observed because of the hydrophilic characteristic of MB, but the initial release rate of **PM-MB** was obviously inhibited. Most drug-loaded nanofibers fabricated by a drug/polymer mixture via single-spinneret electrospinning cause drastic initial drug release owing to the distribution of drugs on the surface and inside of the fibers, and the superficially adsorbed drugs resulted in the initial burst release. Providing interaction (e.g., electrostatic force) between drugs and polymers is conducive to preventing the obvious initial release without any additional chemical modification of drugs or polymers.[44] The electrostatic force between positively charged MB and the MPC moiety provided diffusion resistance and slowed the initial release rate. For **PCL-MB** and **PH-MB**, almost 84.6 ± 4.4 and 94.4 ± 2.1% of loaded MB were released within 12 h after directly exposed to the aqueous medium. The fastest release rate of **PH-MB** presumably was attributed to not only the ionized structure of MB but also the easy stretching and swelling of the hydrophilic PHEMA segment in an aqueous environment, which contributed to an accelerated drug release rate. However, **PM-MB** showed the slowest release rate, and the residual content of MB was around 49.5 ± 3.1% after 12 h (Figure 5b). The sustained MB release profile might be ascribed to the diffusion resistance resulting from the electrostatic attraction


https://doi.org/10.1021/acsomega.3c03964
ACS Omega 2023, 8, 36906−36918

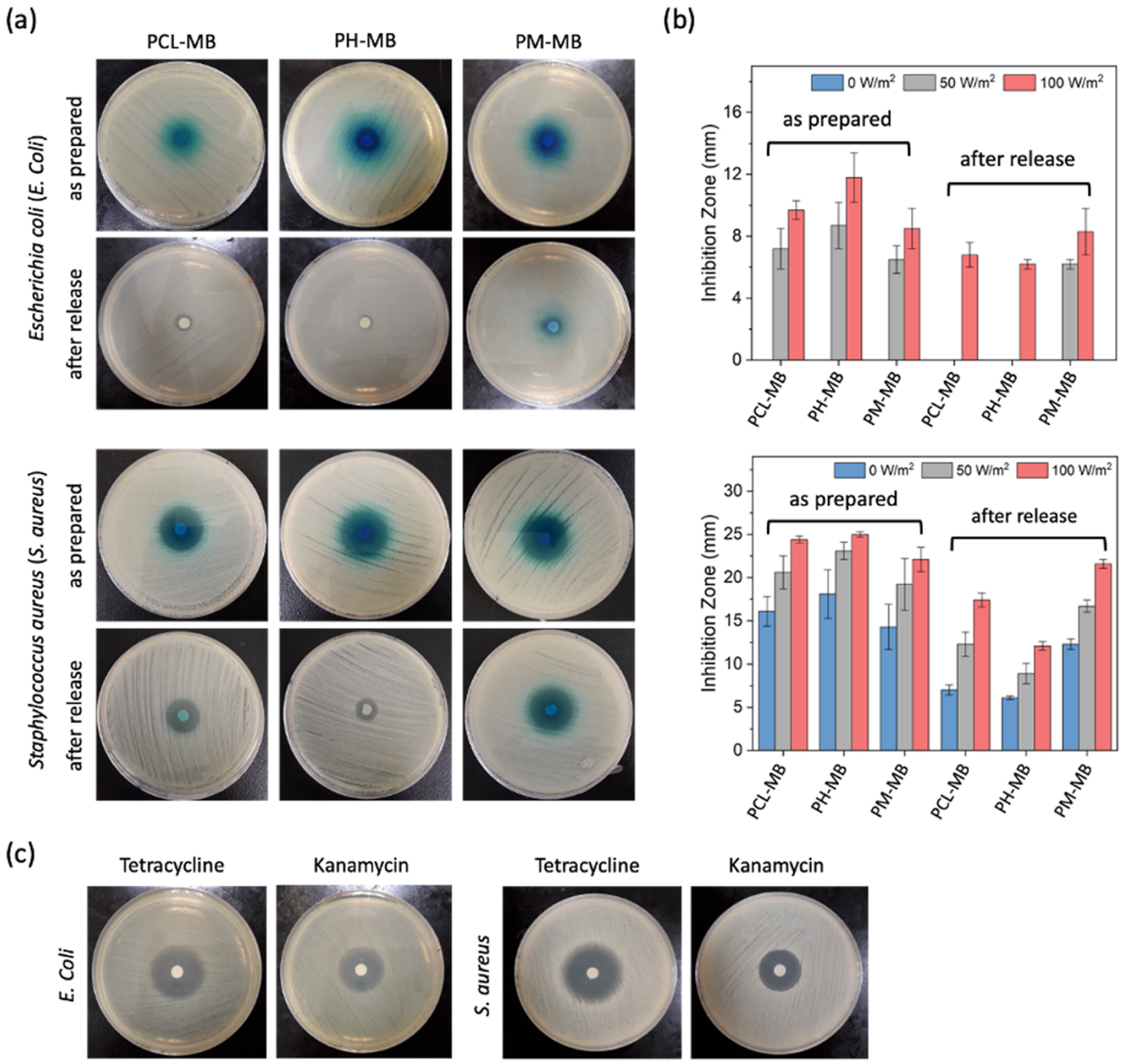


**Figure 6.** Antibacterial photodynamic inactivation evaluation: (a) photographs of inhibition zone test of different MB-loaded nanofibers as prepared as well as after MB release of 12 h inoculated with *E. coli* and *S. aureus* under illumination (100 W $m^{-2}$) for 60 min; (b) inhibition zone test of MB-loaded nanofibers as prepared as well as after MB release of 12 h inoculated with *E. coli* and *S. aureus* in different illumination conditions (0, 50, and 100 W $m^{-2}$) for 60 min; (c) photographs of inhibition zone test of antibiotics (tetracycline and kanamycin) inoculated with *E. coli* and *S. aureus*.

between MB and the zwitterionic PMPC segment, which significantly slowed the release rate. This result indicated the sustained release of MB was beneficial to produce ROS upon illumination at a prolonged time period to act on the bacteria during the use of the nanofibrous dressing and achieve the purpose of long-term bacterial inhibition.

The generation of single oxygen from the MB-loaded nanofibrous mats upon illumination was identified by a SOSG reagent. The SOSG presents a strong green fluorescence when the anthracene moiety reacts with $^1O_2$ and transfers to endoperoxide that prohibits the photoinduced electron transfer. Figure 5c shows the fluorescence variations of SOSG in the absence (plain mats) and in the presence (MB-loaded mats and free MB) of MB over a period of illumination time. The plain mats showed almost no fluorescent signal, suggesting that the singlet oxygen was indeed produced by MB in the presence of light. The fluorescence intensities of MB-loaded mats and free MB progressively increased with illumination time. Free MB showed the best singlet oxygen generation efficiency because it reacted directly with SOSG in an aqueous solution. On the contrary, MB-loaded mats produced less singlet oxygen probably because MB needed to be released from the nanofibers before generating $^1O_2$ or the generated $^1O_2$ required to diffuse out from the nanofibers. Among the MB-loaded mats, the good hydrophilicity of **PH-MB** caused the nanofibers to be swollen, promoting the rapid


https://doi.org/10.1021/acsomega.3c03964
ACS Omega 2023, 8, 36906−36918

release of MB in an aqueous environment and exhibiting better singlet oxygen generation compared with **PCL-MB** and **PM-MB**. Due to the electrostatic attraction between MB and zwitterionic MPC, the slow release of MB from **PM-MB** rendered it to have the lowest singlet oxygen generation efficiency. This result was consistent with the release behaviors. Figure 5d shows the singlet oxygen generation efficiency of MB-loaded mats after 12 h of in vitro release. All MB-loaded nanofibrous mats still produced $^1O_2$ under illumination; however, **PCL-MB** and **PH-MB** with less residual content of MB resulted in a significant decrease in the singlet oxygen generation efficiency. Although **PM-MB** initially showed low singlet oxygen generation efficiency due to the slow release of MB, it still retained 49.5 ± 3.1% content of MB and the highest singlet oxygen generation efficiency after 12 h of release, which proved **PM-MB** had long-lasting antibacterial properties.

**3.4. In Vitro Cytotoxicity and Phototoxicity.** As a protective barrier against external contact, ideal wound dressings should not only provide the above-mentioned appropriate environment to promote wound healing but also should not produce toxicity to normal cells during the use as well as cause secondary damage to the nascent tissue when removed. Furthermore, minimal or even no phototoxicity is another important factor in antibacterial wound dressing through aPDT treatment. The cell viability was evaluated using L929 cells, which were incubated on the surface of MB-loaded nanofibrous mats or free MB for 24 h in the absence and presence of illumination. Cells were seeded on the TCP without any treatment as a control group. As presented in Figure 5e, the cell viability of free MB, plain mats, and MB-loaded mats remained greater than 90% in the absence of illumination. Compared to plain mats, MB-loaded mats revealed a slight effect on cell viability that may be ascribed to the inherent toxicity of the positive charges in the MB molecules.[22,24] This result demonstrated that all the nanofibrous mats have good cytocompatibility and no dark cytotoxicity at the dose of MB used in this study. For the phototoxic study under different illumination conditions (50 and 100 W $m^{-2}$), no apparent cell death was observed in plain mats, suggesting that the light dose used was safe for cells. The cell viability of free MB and MB-loaded mats exhibited a slight decrease as the light dose increased, suggesting that the production of $^1O_2$ by MB upon illumination resulted in minor cellular damage. Nevertheless, the cell viability was still above 80%, which satisfied the noncytotoxic level of the ISO 10993-5 standard. These results confirmed that the MB-loaded nanofibrous mats having low cytotoxicity and good cytocompatibility had great potential for wound dressing applications.

**3.5. Antibacterial Photodynamic Activity.** The antibacterial photodynamic activities of MB-loaded nanofibrous mats against Gram-positive *S. aureus* and Gram-negative *E. coli* were measured by disk-diffusion methods under different illumination conditions. The MB-loaded mats, as well as plain nanofibers as control groups, were evaluated under different illumination doses. The disk-diffusion method provides a qualitative assessment to mimic the real use of nanofibrous mats as dressings or scaffolds at the interface between nanofibers and wounds, which provides valuable antibacterial information. The inhibition zones of all the nanofibrous mats are presented in Figures 6a,b and S2 and S3 (Supporting Information). As expected, no inhibitory activity was detected for the plain mats either in the absence or presence of illumination against *S. aureus* and *E. coli*, indicating that they had no bactericidal activity, and the light dose used was not harmful. All MB-loaded nanofibrous mats against *S. aureus* showed that the inhibition zones around mats increased with increasing light doses. The bactericidal activity was even observed under dark conditions, which might be attributed to the inherent toxicity of MB electrostatically bound and permeated through the outer membrane and/or cytoplasmic membrane of bacteria to achieve a bactericidal effect.[45] Moreover, MB has been reported to achieve bactericidal effect by destroying cell walls, proteins on the cell membranes, and DNA in bacteria, which can be enhanced with increasing light dose.[46,47] The results also confirmed that the generated singlet oxygen resulting from MB upon illumination effectively killed bacteria through aPDT activity. However, the antibacterial activity of all of the MB-loaded mats against *E. coli* was weaker than that against *S. aureus*. No obvious inactivation was observed in the absence of illumination (dark control), indicating no dark toxicity and photodynamic inactivation activity toward Gram-negative bacteria. The different bactericidal activity results from the extra outer membrane of Gram-negative bacteria consisting of lipopolysaccharides that provide a barrier to restrict the diffusion of MB into bacteria cells and further limit the aPDT activity, whereas the Gram-positive bacteria do not have lipopolysaccharides, and the wall structure is loose so that the photosensitizer can easily penetrate.[47,48] This result was consistent with the literature,[20] confirming the lower susceptibility of Gram-negative bacteria toward the most PS and aPDT effects. On the other hand, **PH-MB** had the largest inhibitory zone, while **PM-MB** had the smallest one. The rapid MB release rate of **PH-MB** was conducive to extracellular or intracellular accumulation of MB, which increased the probability of $^1O_2$ acting on bacterial cells. Due to the sustained release profile of **PM-MB**, the disk-diffusion study was also conducted on all of the MB-loaded mats after 12 h of MB release (Figure 6a,b). As expected, all the MB-loaded mats still displayed a better aPDT effect on *S. aureus* than *E. coli*. Although **PH-MB** initially had the best aPDT activity, the inhibition zone was reduced because of less residual MB within the nanofibers after 12 h of release. However, the slow MB release of **PM-MB** allowed it to retain nearly half of the MB residue, thus maintaining a long-lasting and effective inhibitory zone upon illumination even after 12 h of release. This result confirmed that **PM-MB** had a long-lasting aPDT capability. We also compared the inhibition zone of MB-loaded mats with antibiotics, such as tetracycline (27 mm for *S. aureus* and *E. coli*) and kanamycin (21 mm for *E. coli* and 23 mm for *S. aureus*) (Figure 6c). Upon illumination at 100 W $m^{-2}$, all the MB-loaded nanofibrous mats exhibited a similar inhibition zone with the antibiotics against *S. aureus* but less photodynamic inactivation activity against *E. coli*. Although the antibacterial activity of *E. coli*. for current MB-loaded nanofibrous mats was not as high as expected and the reasons were as mentioned above, better photodynamic inactivation of bacteria can be achieved by adjusting the light dose and the concentration of photosensitizer. Overall, the **PM-MB** nanofibers can achieve long-lasting inactivation of both Gram-negative and Gram-positive bacteria through an aPDT treatment and have the potential to be used as antibacterial wound dressings to avoid the use of antibiotics.

## 4. CONCLUSIONS

In summary, the zwitterionic nanofibrous mat loaded with MB as the photosensitizer (**PM-MB**) was successfully fabricated by


https://doi.org/10.1021/acsomega.3c03964
ACS Omega 2023, 8, 36906−36918

electrospinning technology to facilitate both antibiofouling ability and aPDT for wound dressing applications. The **PM** nanofibrous mats exhibited not only promising water absorption ability, water retention capacity, and WVP but also excellent cytocompatibility. The zwitterionic nanofibrous mat (**PM**) showed a better antibiofouling performance against both nonspecific protein and L929 cell adhesion than hydrophobic **PCL** and hydrophilic **PH** nanofibrous mats. In vitro release study showed that the **PM-MB** nanofibrous mat had a slower drug release profile compared to those of **PCL-MB** and **PH-MB**, indicating that the long-lasting release of MB could effectively produce singlet oxygen with a prolonged time profile upon illumination. All MB-loaded nanofibrous mats have shown better aPDT against Gram-positive *S. aureus* than Gram-negative *E. coli* upon moderate illumination because of the lipopolysaccharides contained in the outer membrane of Gram-negative bacteria as an impermeable barrier that limited aPDT activity. The long-lasting release of **PM-MB** confirmed that the nanofibrous mat could effectively and constantly inhibit bacterial proliferation via aPDT. The antibacterial ability of MB-loaded nanofibers was commensurate or slightly inferior to that of antibiotics (e.g., tetracycline and kanamycin), indicating that **PM-MB** could be used as a substitute for antibiotics. Overall, the zwitterionic nanofibrous mat integrated with antibacterial photodynamic inactivation, antibiofouling performance, and long-lasting antibacterial property provided a new pathway to fabricate antibacterial wound dressing applications.

## ■ ASSOCIATED CONTENT

### Supporting Information

The Supporting Information is available free of charge at https://pubs.acs.org/doi/10.1021/acsomega.3c03964.

Synthetic routes and $^1$H NMR spectra for PCL, PCL-*b*-PHEMA, and PCL-*b*-PMPC; photographs of the inhibition zone test of different plain nanofibrous mats; and MB-loaded nanofibrous mats inoculated with *E. coli* and *S. aureus* in the dark or illuminated (PDF)

## ■ AUTHOR INFORMATION


### Corresponding Author

**Ching-Yi Chen** − *Department of Chemical Engineering, National Chung Cheng University, Chia-Yi County 62102, Taiwan;* orcid.org/0000-0001-6103-9468; Email: chmcyc@ccu.edu.tw; Fax: +886 05 2727 1206

### Author

**Wen-Yen Chang** − *Department of Chemical Engineering, National Chung Cheng University, Chia-Yi County 62102, Taiwan*

Complete contact information is available at: https://pubs.acs.org/10.1021/acsomega.3c03964


### Author Contributions

The manuscript was written through contributions of both authors. Both authors have given approval to the final version of the manuscript.

### Notes

The authors declare no competing financial interest.

## ■ ACKNOWLEDGMENTS

The financial support from the Ministry of Science and Technology of Taiwan is highly appreciated (MOST 109-2221-E-194-045). The authors acknowledge Dr Kuang-Tse Huang (Department of Chemical Engineering, National Chung Cheng University) and Dr Bing-Mu Hsu (Department of Earth and Environmental Sciences, National Chung Cheng University) for their help and support in providing the bacterial strains and culture.

## ■ REFERENCES


(1) Zeng, Q.; Qi, X.; Shi, G.; Zhang, M.; Haick, H. Wound Dressing: From Nanomaterials to Diagnostic Dressings and Healing Evaluations. *ACS Nano* **2022**, *16*, 1708−1733.

(2) Ghomi, E. R.; Khalili, S.; Khorasani, S. N.; Neisiany, R. E.; Ramakrishna, S. Wound Dressings: Current Advances and Future Directions. *J. Appl. Polym. Sci.* **2019**, *136*, 47738.

(3) Sheokand, B.; Vats, M.; Kumar, A.; Srivastava, C. M.; Bahadur, I.; Pathak, S. R. Natural Polymers Used in the Dressing Materials for Wound Healing: Past, Rresent and Future. *J. Polym. Sci.* **2023**, *61*, 1389.

(4) Liu, M.; Duan, X. P.; Li, Y. M.; Yang, D. P.; Long, Y. Z. Electrospun Nanofibers for Wound Healing. *Mater. Sci. Eng., C* **2017**, *76*, 1413−1423.

(5) Gao, C.; Zhang, L.; Wang, J.; Jin, M.; Tang, Q.; Chen, Z.; Cheng, Y.; Yang, R.; Zhao, G. Electrospun Nanofibers Promote Wound Healing: Theories, Techniques, and Perspectives. *J. Mater. Chem. B* **2021**, *9*, 3106−3130.

(6) Sethuram, L.; Thomas, J. Therapeutic Applications of Electrospun Nanofibers Impregnated with Various Biological Macromolecules for Effective Wound Healing Strategy - A Review. *Biomed. Pharmacother.* **2023**, *157*, 113996.

(7) Mao, Y.; Shen, W.; Wu, S.; Ge, X.; Ao, F.; Ning, Y.; Luo, Y.; Liu, Z. Electrospun Polymers: Using Devices to Enhance Their Potential for Biomedical Applications. *React. Funct. Polym.* **2023**, *186*, 105568.

(8) Ambekar, R. S.; Kandasubramanian, B. Advancements in Nanofibers for Wound Dressing: A Review. *Eur. Polym. J.* **2019**, *117*, 304−336.

(9) Li, M.; Chen, J.; Shi, M.; Zhang, H.; Ma, P. X.; Guo, B. Electroactive Anti-oxidant Polyurethane Elastomers with Shape Memory Property as Non-adherent Wound Dressing to Enhance Wound Healing. *Chem. Eng. J.* **2019**, *375*, 121999.

(10) Grainger, D. W. All Charged Up About Implanted Biomaterials. *Nat. Biotechnol.* **2013**, *31*, 507−509.

(11) Zhang, Y.; Liu, Y.; Ren, B.; Zhang, D.; Xie, S.; Chang, Y.; Yang, J.; Wu, J.; Xu, L.; Zheng, J. Fundamentals and Applications of Zwitterionic Antifouling Polymers. *J. Phys. D: Appl. Phys.* **2019**, *52*, 403001.

(12) Ozcan, S.; Kaner, P.; Thomas, D.; Cebe, P.; Asatekin, A. Hydrophobic Antifouling Electrospun Mats from Zwitterionic Amphiphilic Copolymers. *ACS Appl. Mater. Interfaces* **2018**, *10*, 18300−18309.

(13) Feng, Y.; Wang, Q.; He, M.; Zhao, W.; Liu, X.; Zhao, C. Nonadherent Zwitterionic Composite Nanofibrous Membrane with a Halloysite Nanocarrier for Sustained Wound Anti-Infection and Cutaneous Regeneration. *ACS Biomater. Sci. Eng.* **2020**, *6*, 621−633.

(14) Ghorbani, J.; Rahban, D.; Aghamiri, S.; Teymouri, A.; Bahador, A. Photosensitizers in Antibacterial Photodynamic Therapy: An Overview. *Laser Ther.* **2018**, *27*, 293−302.

(15) Hamblin, M. R. Antimicrobial Photodynamic Inactivation: A Bright New Technique to Kill Resistant Microbes. *Curr. Opin. Microbiol.* **2016**, *33*, 67−73.

(16) Dias, L. M.; Ferrisse, T. M.; Medeiros, K. S.; Cilli, E. M.; Pavarina, A. C. Use of Photodynamic Therapy Associated with Antimicrobial Peptides for Bacterial Control: A Systematic Review and Meta-Analysis. *Int. J. Mol. Sci.* **2022**, *23*, 3226.

(17) Kashef, N.; Huang, Y. Y.; Hamblin, M. R. Advances in Antimicrobial Photodynamic Inactivation at the Nanoscale. *Nanophotonics* **2017**, *6*, 853−879.
(18) Maisch, T.; Baier, J.; Franz, B.; Maier, M.; Landthaler, M.; Szeimies, R. M.; Bäumler, W. The Role of Singlet Oxygen and Oxygen Concentration in Photodynamic Inactivation of Bacteria. *Proc. Natl. Acad. Sci. U.S.A.* **2007**, *104*, 7223−7228.
(19) Fuchs, J.; Thiele, J. The Role of Oxygen in Cutaneous Photodynamic Therapy. *Free Radical Biol. Med.* **1998**, *24*, 835−847.
(20) Preis, E.; Anders, T.; Širc, J.; Hobzova, R.; Cocarta, A.-I.; Bakowsky, U.; Jedelská, J. Biocompatible Indocyanine Green loaded PLA Nanofibers for in Situ Antimicrobial Photodynamic Therapy. *Mater. Sci. Eng., C* **2020**, *115*, 111068.
(21) Abdel Khalek, M. A.; Abdel Gaber, S. A.; El-Domany, R. A.; El-Kemary, M. A. Photoactive Electrospun Cellulose Acetate/Polyethylene Oxide/Methylene Blue and Trilayered Cellulose Acetate/Polyethylene Oxide/Silk Fibroin/Ciprofloxacin Nanofibers for Chronic Wound Healing. *Int. J. Biol. Macromol.* **2021**, *193*, 1752−1766.
(22) Wainwright, M.; Crossley, K. B. Methylene Blue - A Therapeutic Dye for All Seasons? *Aust. J. Chem.* **2002**, *14*, 431−443.
(23) Darabpour, E.; Kashef, N.; Mashayekhan, S. Chitosan Nanoparticles Enhance the Efficiency of Methylene Blue-mediated Antimicrobial Photodynamic Inactivation of Bacterial Biofilms: An In Vitro Study. *Photodiagn. Photodyn. Ther.* **2016**, *14*, 211−217.
(24) Usacheva, M. N.; Teichert, M. C.; Biel, M. A. Comparison of the Methylene Blue and Toluidine Blue Photobactericidal Efficacy Against Gram-Positive and Gram-Negative Microorganisms. *Lasers Surg. Med.* **2001**, *29*, 165−173.
(25) Saeed, A. O.; Dey, S.; Howdle, S. M.; Thurecht, K. J.; Alexander, C. One-pot Controlled Synthesis of Biodegradable and Biocompatible Co-polymer Micelles. *J. Mater. Chem.* **2009**, *19*, 4529−4535.
(26) Samadian, H.; Zamiri, S.; Ehterami, A.; Farzamfar, S.; Vaez, A.; Khastar, H.; Alam, M.; Ai, A.; Derakhshankhah, H.; Allahyari, Z.; Goodarzi, A.; Salehi, M. Electrospun Cellulose Acetate/Gelatin Nanofibrous Wound Dressing Containing Berberine for Diabetic Foot Ulcer Healing: In Vitro and In Vivo Studies. *Sci. Rep.* **2020**, *10*, 8312.
(27) Niu, Z.; Zhao, Y.; Sun, W.; Shi, S.; Gong, Y. Biomimetic Surface Modification of Polypropylene by Surface Chain Transfer Reaction Based on Mussel-inspired Adhesion Technology and Thiol Chemistry. *Appl. Surf. Sci.* **2016**, *386*, 41−50.
(28) Huang, K. T.; Fang, Y. L.; Hsieh, P. S.; Li, C.-C.; Dai, N. T.; Huang, C. J. Zwitterionic Nanocomposite Hydrogels as Effective Wound Dressings. *J. Mater. Chem. B* **2016**, *4*, 4206−4215.
(29) Zhang, M.; Yu, P.; Xie, J.; Li, J. Recent Advances of Zwitterionic-based Topological Polymers for Biomedical Applications. *J. Mater. Chem. B* **2022**, *10*, 2338−2356.
(30) Shenoy, S. L.; Bates, W. D.; Frisch, H. L.; Wnek, G. E. Role of Chain Entanglements on Fiber Formation During Electrospinning of Polymer Solutions: Good Solvent, Non-specific Polymer-polymer Interaction limit. *Polymer* **2005**, *46*, 3372−3384.
(31) Brown, R. H.; Hunley, M. T.; Allen, M. H., Jr; Long, T. E. Electrospinning Zwitterion-Containing Nanoscale Acrylic Fibers. *Polymer* **2009**, *50*, 4781−4787.
(32) Li, Y. L.; Chen, C. Y. Near-Infrared Light-Remote Localized Drug Delivery Systems Based on Zwitterionic Polymer Nanofibers for Combination Therapy. *Polymers* **2022**, *14*, 1860.
(33) Chen, H.; Lan, G.; Ran, L.; Xiao, Y.; Yu, K.; Lu, B.; Dai, F.; Wu, D.; Lu, F. A Novel Wound Dressing Based on a Konjac Glucomannan/Silver Nanoparticle Composite Sponge Effectively Kills Bacteria and Accelerates Wound Healing. *Carbohydr. Polym.* **2018**, *183*, 70−80.
(34) Raafat, A. I.; El-Sawy, N. M.; Badawy, N. A.; Mousa, E. A.; Mohamed, A. M. Radiation Fabrication of Xanthan-based Wound Dressing Hydrogels Embedded ZnO Nanoparticles: In Vitro Evaluation. *Int. J. Biol. Macromol.* **2018**, *118*, 1892−1902.
(35) Junker, J. P.; Kamel, R. A.; Caterson, E. J.; Eriksson, E. Clinical Impact Upon Wound Healing and Inflammation in Moist, Wet, and Dry Environments. *Adv. Wound Care* **2013**, *2*, 348−356.
(36) Saeed, S. M.; Mirzadeh, H.; Zandi, M.; Barzin, J. Designing and Fabrication of Curcumin Loaded PCL/PVA Multi-layer Nanofibrous Electrospun Structures as Active Wound Dressing. *Prog. Biomater.* **2017**, *6*, 39−48.
(37) Roach, P.; Farrar, D.; Perry, C. C. Interpretation of Protein Adsorption: Surface-induced Conformational Changes. *J. Am. Chem. Soc.* **2005**, *127*, 8168−8173.
(38) He, Y.; Hower, J.; Chen, S.; Bernards, M. T.; Chang, Y.; Jiang, S. Molecular Simulation Studies of Protein Interactions with Zwitterionic Phosphorylcholine Self-Assembled Monolayers in the Presence of Water. *Langmuir* **2008**, *24*, 10358−10364.
(39) Mollahosseini, A.; Abdelrasoul, A.; Shoker, A. Latest Advances in Zwitterionic Structures Modified Dialysis Membranes. *Mater. Today Chem.* **2020**, *15*, 100227.
(40) Fujishita, S.; Inaba, C.; Tada, S.; Gemmei-Ide, M.; Kitano, H.; Saruwatari, Y. Effect of Zwitterionic Polymers on Wound Healing. *Biol. Pharm. Bull.* **2008**, *31*, 2309−2315.
(41) Liu, P. S.; Chen, Q.; Wu, S. S.; Shen, J.; Lin, S. C. Surface Modification of Cellulose Membranes with Zwitterionic Polymers for Resistance to Protein Adsorption and Platelet Adhesion. *J. Membr. Sci.* **2010**, *350*, 387−394.
(42) Stoll, K. R.; Scholle, F.; Zhu, J.; Zhang, X.; Ghiladi, R. A. BODIPY-Embedded Electrospun Materials in Antimicrobial Photodynamic Inactivation. *Photochem. Photobiol. Sci.* **2019**, *18*, 1923−1932.
(43) Guo, F. C.; Chen, C. Y. Zwitterionic Core-Sheath Nanofibers in Antibacterial Photodynamic Therapy. *ACS Appl. Polym. Mater.* **2022**, *4*, 4576−4587.
(44) Mauri, E.; Chincarini, G. M. F.; Rigamonti, R.; Magagnin, L.; Sacchetti, A.; Rossi, F. Modulation of Electrostatic Interactions to Improve Controlled Drug Delivery from Nanogels. *Mater. Sci. Eng., C* **2017**, *72*, 308−315.
(45) Hussain, S.; Harris, F.; Phoenix, D. A. The Phototoxicity of Phenothiazinium-based Photosensitizers to Bacterial Membranes. *FEMS Immunol. Med. Microbiol.* **2006**, *46*, 124−130.
(46) Goulart, R. C.; Thedei, G., Jr.; Souza, S. L. S.; Tedesco, A. C.; Ciancaglini, P. Comparative Study of Methylene Blue and Erythrosine Dyes Employed in Photodynamic Therapy for Inactivation of Planktonic and Biofilm-cultivated Aggregatibacter Actinomycetemcomitans. *Photomed. Laser Surg.* **2010**, *28*, S-85.
(47) Liu, Y.; Qin, R.; Zaat, S. A. J.; Breukink, E.; Heger, M. Antibacterial Photodynamic Therapy: Overview of a Promising Approach to Fight Antibiotic-resistant Bacterial Infections. *J. Clin. Transl. Res.* **2015**, *1*, 140−167.
(48) Kashef, N.; Huang, Y. Y.; Hamblin, M. R. Advances in Antimicrobial Photodynamic Inactivation at the Nanoscale. *NANO* **2017**, *6*, 853−879.


https://doi.org/10.1021/acsomega.3c03964
*ACS Omega* 2023, 8, 36906−36918